

Supplementary Information

Oxime organic cathode materials for long-lifespan lithium-ion batteries

Luchen Jia,^a Pengli Bao^b, Zehui Fan^a, Yuansheng Liu^a, Sitong Yao^a and Yunhua Xu^{*a}

^a School of Materials Science and Engineering, and State Key Laboratory of Advanced Materials for Intelligent Sensing, Tianjin University, Tianjin 300072, China

^b Department of Chemistry, and Tianjin Key Laboratory of Molecular Optoelectronic Science, Tianjin University, Tianjin 300072, China

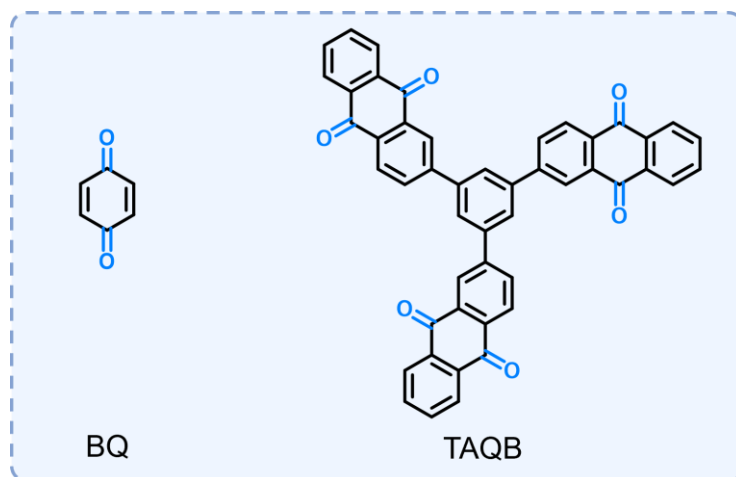


Fig. S1 Molecular structures of BQ and TAQB.

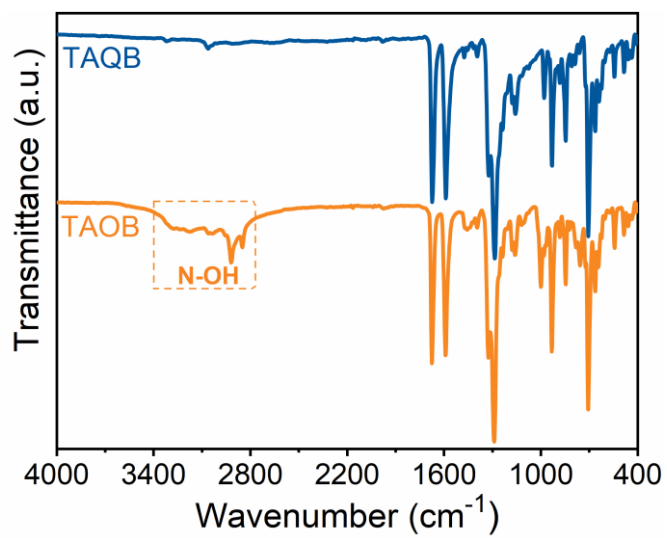


Fig. S2 FTIR spectra of TAQB and TAQB.

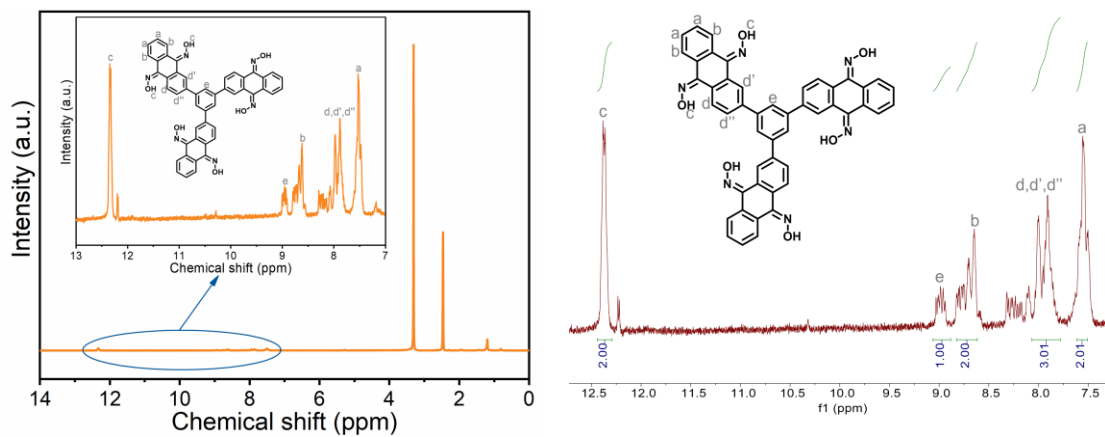


Fig. S3 ^1H NMR spectrum of TAOB in $(\text{CD}_3)_2\text{SO}$.

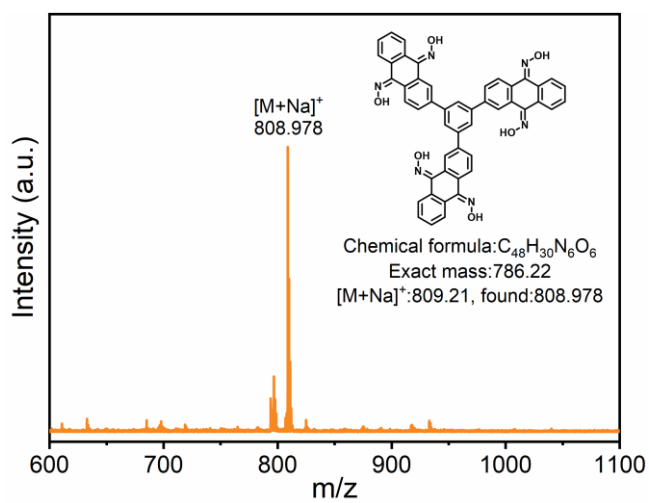


Fig. S4 MALDI-TOF-MS spectrum of TAOB.

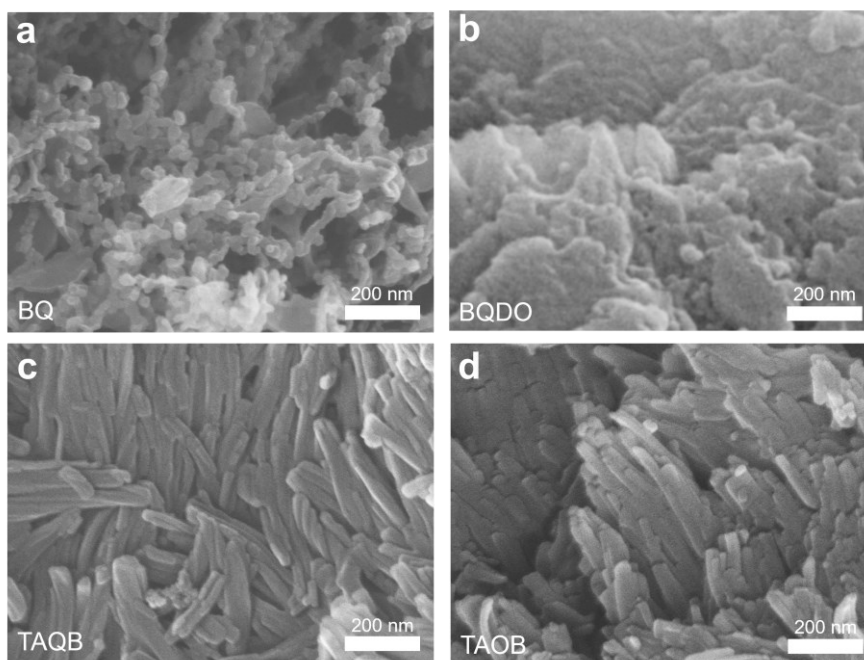


Fig. S5 SEM images at high magnification of BQ, BQDO, TAQB and TAOB.

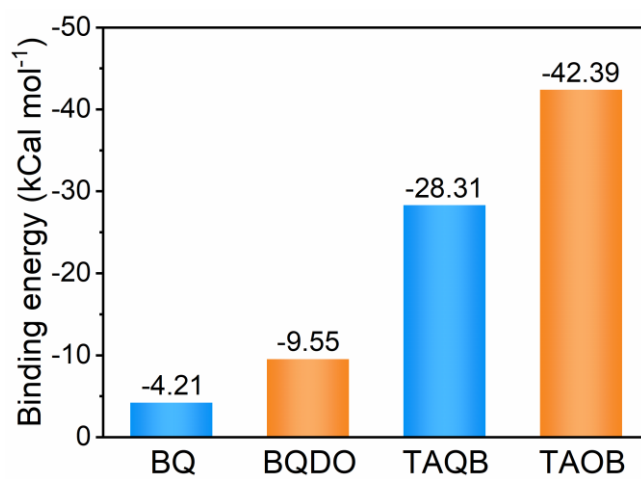
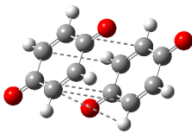
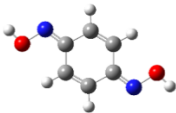
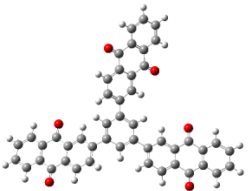
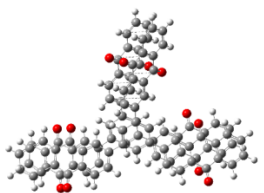
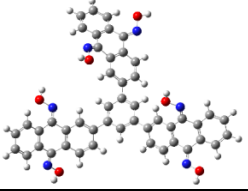
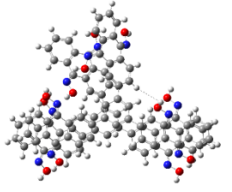


Fig. S6 Comparison of binding energies of BQ, BQDO, TAQB and TAOB.

Table S1. Binding energies of BQ, BQDO, TAQB and TAOB.

Compounds	Geometrical configuration	Single point energy (Ha)	Binding energy (Ha)	Binding energy (kCal mol ⁻¹)
BQ		-381.400530		
			-0.006710	-4.21
2BQ		-762.807770		
BQDO		-491.994937		
			-0.015223	-9.55
2BQDO		-984.005097		
TAQB		-2294.825704		
			-0.045115	-28.31
2TAQB		-4589.696523		
TAOB		-2626.516030		
			-0.067548	-42.39
2TAOB		-5253.099608		

The calculation of the binding energy was performed as follows. First, geometrical optimization and frequency calculation were carried out using the B3LYP functional with the 6-31G(d,p) basis set. The "em=GD3BJ" keyword was applied to obtain the optimized molecular structure. Based on this, energy calculations were performed using the higher-level M05-2X functional and the 6-31G* basis set to obtain the single-point energy of the molecules. When two molecules are in close proximity, a non-covalent interaction occurs, and the binding energy can be determined by calculating the energy of the composite system minus the energy of the respective monomers. The binding energy is calculated using the equation with BQ as an example:

$$E_{binding}(BQ) = E(2BQ) - 2 * E(BQ)$$

where $E_{binding}(BQ)$ is the binding energy between two BQ molecules, $E(2BQ)$ is the single point energy of two BQ molecules interacting together, and $E(BQ)$ is the single point energy of a single BQ molecule. The unit conversion is 1 Ha = 627.51 kCal mol⁻¹.

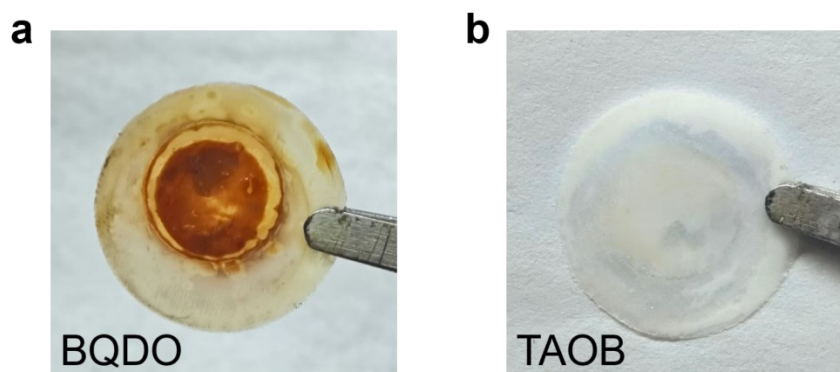


Fig. S7 Optical photographs of the separators removed from the batteries of (a) BQDO and (b) TAOB after 5 cycles.

The obvious color on the surface of the separator in BQDO batteries indicates that the BQDO active material in the electrodes will gradually dissolve during battery operation, leading to a decrease in specific capacity. In contrast, there is no color on the surface of the separator in TAOB batteries, which is one reason for the cycle stability of TAOB batteries.

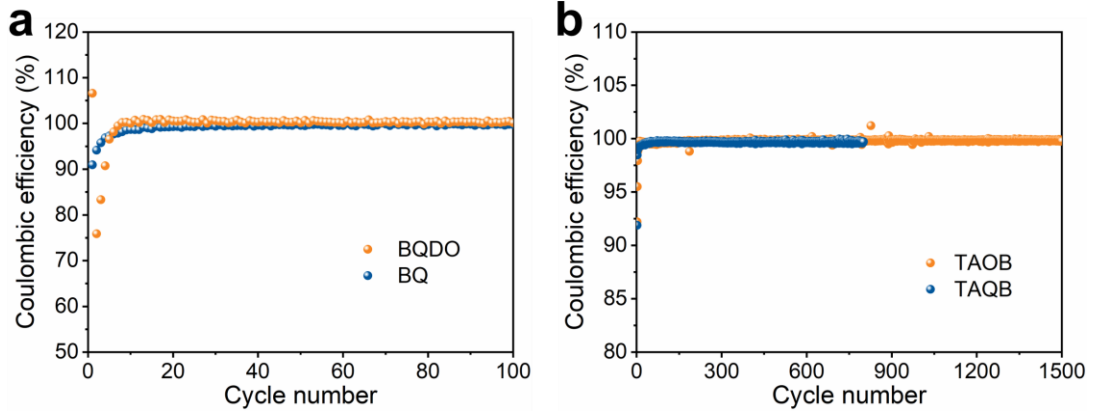


Fig. S8 Corresponding coulombic efficiency of (a) BQDO and BQ, (b) TAOB and TAQB during the charge-discharge cycle at 100 mA g⁻¹ in Fig. 3e,f.

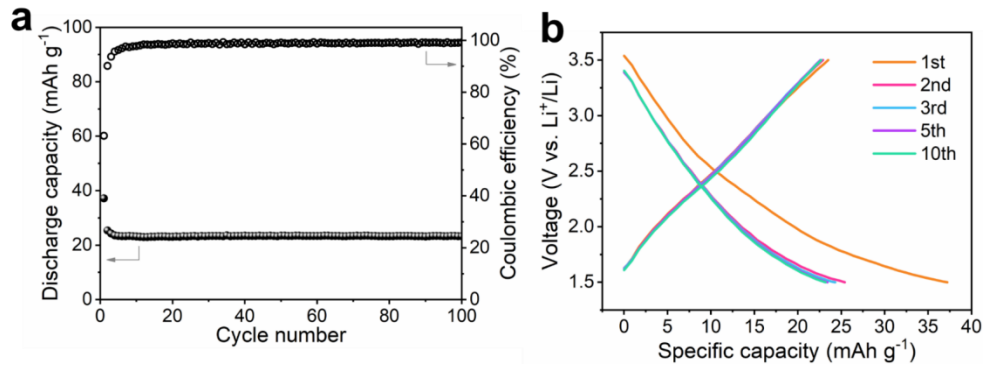


Fig. S9 (a) Cyclic performance of graphene electrode (GR:PVDF = 85:15) at 100 mA g⁻¹ with a potential range of 1.5 to 3.5 V and (b) corresponding charge-discharge curves.

If the electrode composition is AM/GR/PVDF = x:y:1 (AM refers to active material), the actual capacity of active material can be calculated according to the following equations:

$$x C = x C_{AM} + y C_{GR}$$

$$C_{AM} = C - \frac{y}{x} C_{GR}$$

where C is the apparent specific capacity based on the weight of AM, C_{AM} and C_{GR} are the actual specific capacity of AM and GR, and y/x C_{GR} can be regarded as the capacity contribution of GR to the electrode. In Fig. S9, C_{GR} is approximately 24 mAh g⁻¹. Therefore, for the electrode with composition of AM/GR/PVDF = 6:3:1 (x = 6, y = 3),

$$C_{AM} = C - \frac{3}{6} C_{GR} = C - 12 \text{ mAh g}^{-1}$$

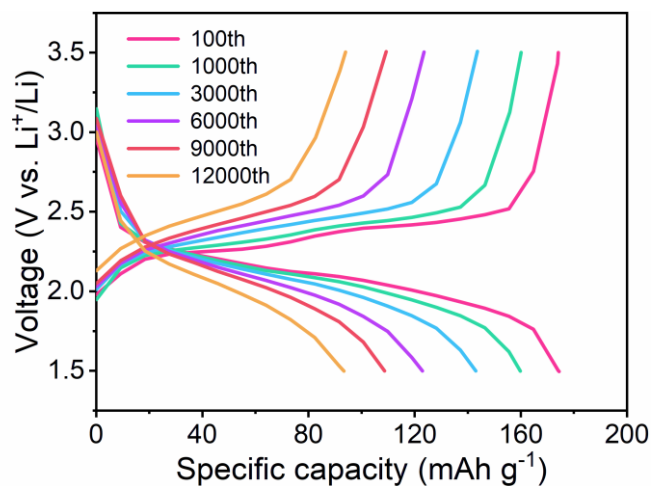


Fig. S10 Charge-discharge curves of TAOB electrode at a current density of 1 A g^{-1} for different number of cycles.

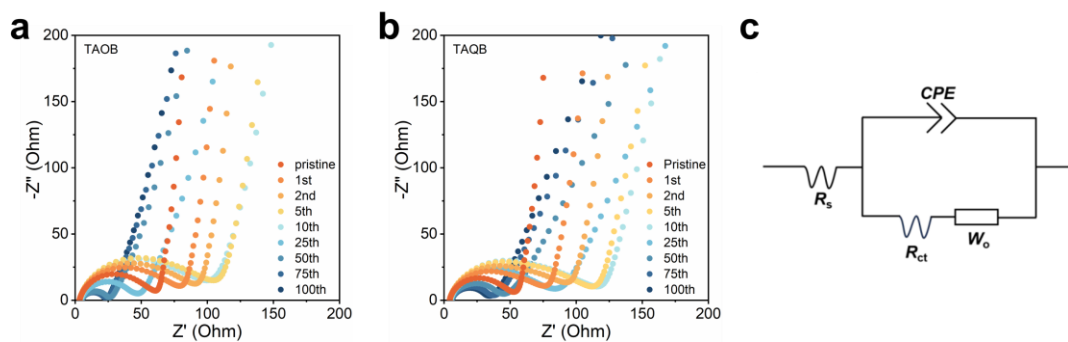


Fig. S11 Nyquist plots of the TAOB (a) and TAQB (b) electrodes after different cycles. (c) Equivalent circuit diagram.

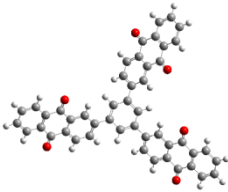
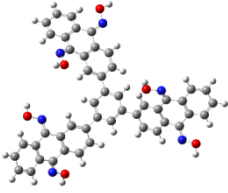
Table S2. Fitted parameter data for equivalent circuit diagrams of TAOB.

State	R_s (Ω)	R_{ct} (Ω)	$CPE-T$	$CPE-P$	W_{O-R}	W_{O-T}	W_{O-P}
Pristine	3.277	50.42	9.0339×10^{-6}	0.86012	37.79	0.13257	0.48039
1st	3.187	65.35	1.0622×10^{-5}	0.84205	56.67	0.18331	0.47533
2nd	3.192	74.92	1.0945×10^{-5}	0.83683	65.06	0.21593	0.47372
5th	3.279	85.79	1.0558×10^{-5}	0.8362	83.03	0.29388	0.46604
10th	3.803	80.66	9.7839×10^{-6}	0.84187	92.53	0.34324	0.45575
25th	4.422	37.15	1.1007×10^{-5}	0.82478	46.66	0.53005	0.42373
50th	4.817	18.66	1.1041×10^{-5}	0.82088	23.97	0.39056	0.41267
75th	4.984	16.81	9.9746×10^{-6}	0.82473	18.06	0.2939	0.41815
100th	5.183	16.15	7.3365×10^{-6}	0.84931	17.63	0.31325	0.41873

Table S3. Fitted parameters in the equivalent circuits of the EIS data for TAQB.

State	R_s (Ω)	R_{ct} (Ω)	$CPE-T$	$CPE-P$	W_{O-R}	W_{O-T}	W_{O-P}
Pristine	4.152	43.15	1.0157×10^{-5}	0.85289	35.60	0.15564	0.47712
1st	3.933	61.14	1.4742×10^{-5}	0.81559	59.49	0.25368	0.46955
2nd	3.876	74.69	1.6332×10^{-5}	0.80353	74.78	0.3273	0.46934
5th	3.788	93.31	2.2270×10^{-5}	0.77302	75.12	2.387	0.45025
10th	4.207	95.86	2.3781×10^{-5}	0.76699	76.01	3.579	0.43178
25th	4.673	68.40	2.3441×10^{-5}	0.77059	66.91	2.439	0.38984
50th	5.475	34.08	1.4508×10^{-5}	0.81453	42.71	1.010	0.36484
75th	5.819	27.29	1.1592×10^{-5}	0.83515	33.18	0.69954	0.37809
100th	5.967	24.91	1.109×10^{-5}	0.83775	30.78	0.67682	0.3873

Table S4. Calculation of free energies of dissolution of TAQB and TAOB.

Molecule name	Geometrical configuration	E_{gas} (Ha)	E_{THF} (Ha)	$\Delta G_{\text{dissolve}}$ (Ha)	$\Delta G_{\text{dissolve}}$ (kCal mol ⁻¹)
TAQB		-2294.824164	-2294.883177	-0.059013	-37.03
TAOB		-2626.514910	-2626.573307	-0.058397	-36.64

The calculation of the free energy of dissolution was carried out as follows. THF was chosen as the solvent environment for the theoretical calculations because the dielectric constant of THF is close to that of DOL-DME when mixed at a volume ratio of 1:1 [$\epsilon_{\text{THF}} = 7.43$, $\epsilon_{\text{DOL}} = 7.1$, $\epsilon_{\text{DME}} = 7.2$, $\epsilon_{\text{DOL-DME}} = (7.1 + 7.2)/2 = 7.15$], which may reflect the immersion of the organic electrode material in the electrolyte during battery testing.

First, geometrical optimizations and frequency calculations were performed using the B3LYP general function, 6-31G (d,p) basis set and THF as the solvent environment to obtain the optimised molecular structure. On this basis, energy calculations were performed using the higher level M05-2X general function, 6-31G* basis set, with or without simulation of the THF solvent environment, to obtain the sum of the electronic energies of the molecules (E_{THF} and E_{gas}) in the solvent and gas environments. The free energy of dissolution is obtained by subtracting the electron energy in the solvent environment from the electron energy in the gas phase environment ($\Delta G_{\text{dissolve}} = E_{\text{THF}} - E_{\text{gas}}$). The unit conversion relationship is 1 Ha = 627.51 kCal mol⁻¹.

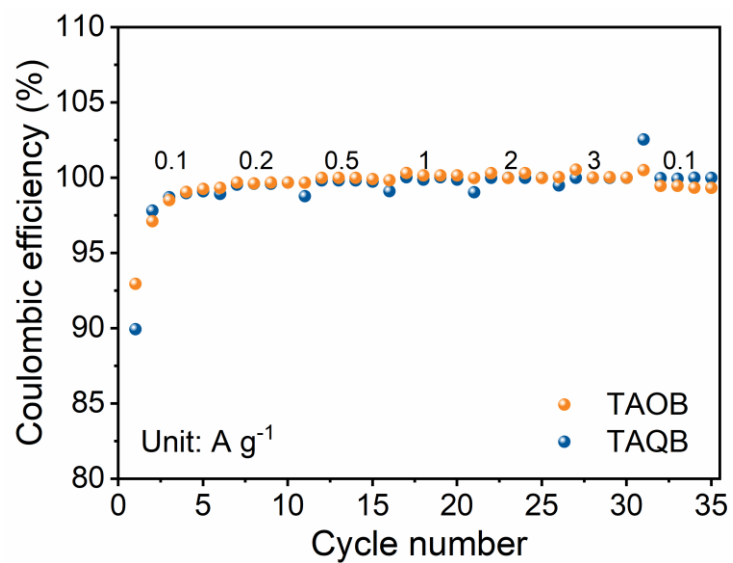


Fig. S12 Coulombic efficiency of TAOB and TAQB in rate performance in Fig. 5a.

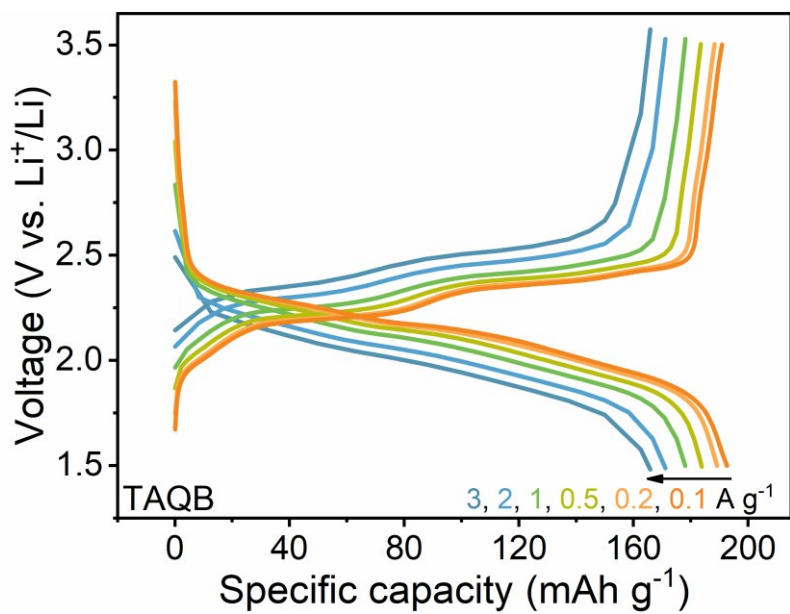


Fig. S13 Charge/discharge curves of TAQB at different current densities.

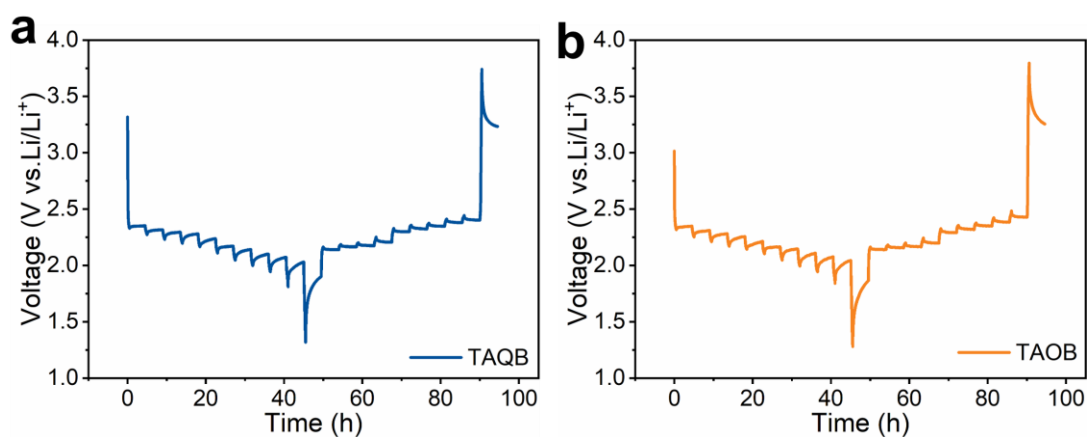


Fig. S14 GITT curves of (a) TAQB and (b) TAOB using the 1 M LiTFSI/DOL-DME (1:1, V:V) electrolyte (1.5–3.5 V, 100 mA g⁻¹, relaxing for 4 h after each discharge/charge step of 30 min).

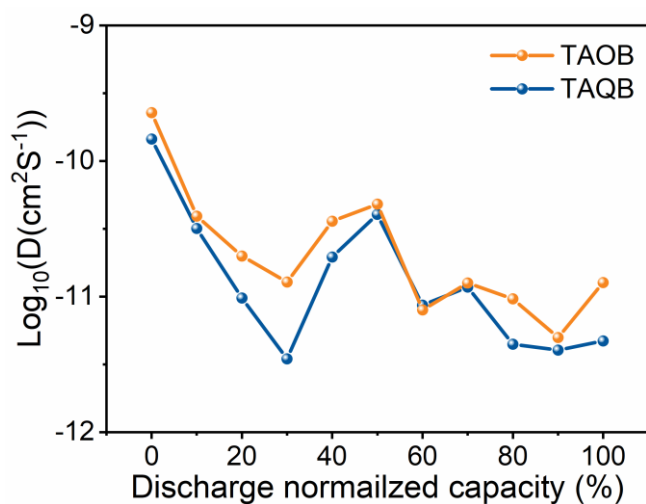


Fig. S15 Diffusion coefficient of lithium ions at discharge state calculated from the GITT data in Fig. S14.

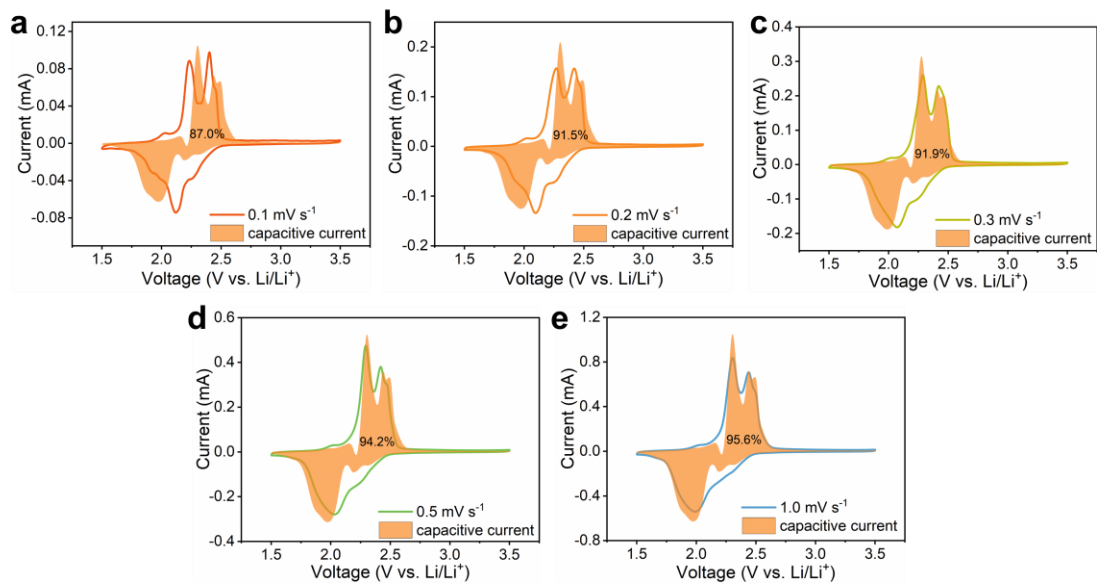


Fig. S16 CV curves and capacity contribution ratios at different scan rates of the TAOB electrode.

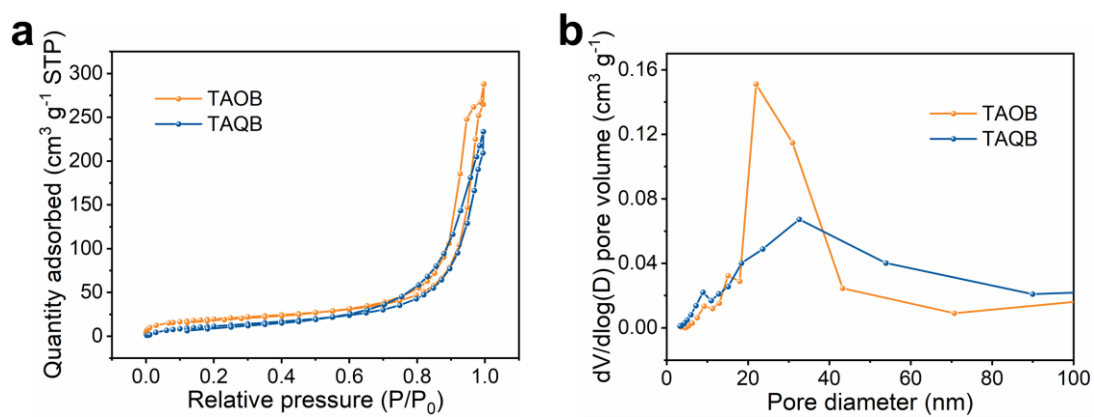


Fig. S17 (a) N_2 adsorption/desorption isotherms and (b) pore size distributions of TAOB and TAQB.

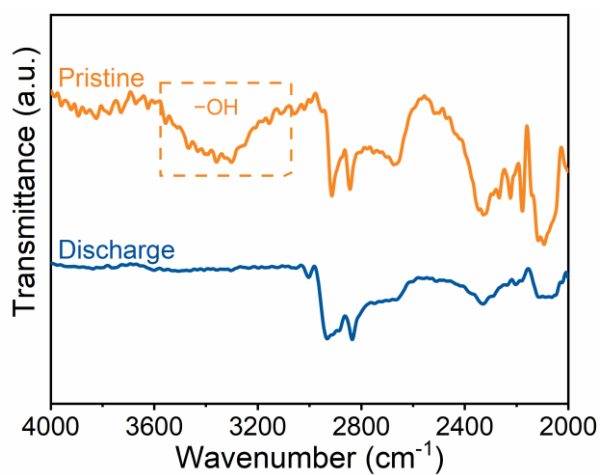


Fig. S18 FTIR spectra of pristine and discharged TAOB electrodes.

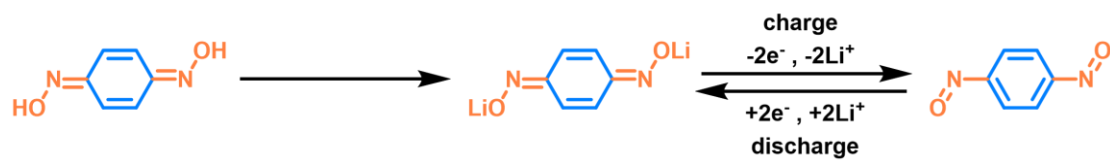


Fig. S19 Illustration of the redox storage mechanism of BQDO in LIBs.